Available online at www.sciencedirect.com

SCIENCE DIRECT®

Earth and Planetary Science Letters 235 (2005) 283–301

EPSL

www.elsevier.com/locate/epsl

# Time variations of land water storage from an inversion of 2 years of GRACE geoids

G. Ramillien[a,*], F. Frappart[a], A. Cazenave[a], A. Güntner[b]

[a] *LEGOS, 14 Avenue Edouard Belin, 31401 Toulouse Cedex 09, France*
[b] *GeoForschungsZentrum (GFZ), Telegrafenberg, Potsdam, Germany*

Received 1 December 2004; received in revised form 25 March 2005; accepted 5 April 2005
Available online 1 June 2005
Editor: V. Courtillot

**Abstract**

By delivering monthly maps of the gravity field, the GRACE project allows the determination of tiny time variations of the Earth's gravity and particularly the effects of fluid mass redistributions at the surface of the Earth. However, GRACE data represent vertically integrated gravity measurements, thus are the sum of all mass redistributions inside the Earth's system (atmosphere, oceans and continental water storage, plus solid Earth). In this paper, we apply a generalized least-squares inverse approach, previously developed by [1] [G. Ramillien, A. Cazenave, O. Brunau, Global time-variations of hydrological signals from GRACE satellite gravimetry, Geophys. J. Int. 158 (2004) 813–826.], to estimate, from the monthly GRACE geoids, continental water storage variations (and their associated uncertainties) over a 2-year time span (April 2002 to May 2004). Tests demonstrating the robustness of the method are presented, including the separation between liquid water reservoirs (surface waters + soil moisture + groundwaters) and snow pack contributions. Individual monthly solutions of total land water storage from GRACE, with a spatial resolution of ~660 km, are presented for the 2-year time span. We also derive the seasonal cycle map. We further estimate water volume changes over eight large river basins in the tropics and compare with model predictions. Finally, we attempt to estimate an average value of the evapotranspiration over each river basin, using the water balance equation which links temporal change in water volume to precipitation, evapotranspiration and runoff. Amplitudes of the GRACE-derived evapotranspiration are regionally consistent to the predictions of global hydrological models.


*Keywords:* GRACE satellite gravimetry; global hydrology; least-squares inversion

## 1. Introduction

In March 2002, a new generation of gravity missions was launched: the Gravity Recovery and Climate Experiment (GRACE) space mission [2,3]. The

* Corresponding author. Tel.: +33 5 61 33 29 34.
*E-mail address:* ramillie@notos.cst.cnes.fr (G. Ramillien).

0012-821X/$ - see front matter © 2005 Elsevier B.V. All rights reserved.
doi:10.1016/j.epsl.2005.04.005

objective of GRACE is to measure spatio-temporal variations of the gravity field with an unprecedented resolution and precision, over time scales ranging from a few months to several years. As gravity is an integral of mass, these spatio-temporal gravity variations represent horizontal mass redistributions only to the extent that they are assumed to be caused by surface loads. On time scales from months to decades, mass redistribution mainly occurs inside the surface fluid envelopes (oceans, atmosphere, ice caps, continental reservoirs) and is related to climate variability. The main application of GRACE is quantifying the terrestrial hydrological cycle through measurements of vertically-integrated water mass changes inside aquifers, soil, surface reservoirs and snow pack, with a precision of a few millimeters in terms of water height and a spatial resolution of ~400 km [4,5].

Until the launch of GRACE, no direct measurements of time-varying storage of snow, soil and underground waters were available globally. Therefore, the global distribution and spatio-temporal changes of land water mass were essentially estimated from modelling. The main motivation for developing global land surface models (LSMs) over the recent decades was to provide realistic temperature and humidity boundary conditions to atmospheric models developed for climate modelling. In effect, many land surface parameters exert a strong influence on water and energy surface fluxes and as a consequence on the atmosphere. Among these parameters, soil moisture and snow mass are important since they affect low-atmosphere state on both short and long (seasonal and inter-annual) time scales. Besides, land water storage and snow mass are themselves affected by atmospheric conditions and climate variability. In the recent years, a number of state-of-the-art LSMs have provided global gridded time series of soil water, underground water and snow mass, typically on a monthly basis and a geographical resolution of $\sim 1^\circ \times 1^\circ$ (among others, [6–11]). These global hydrological data sets are currently derived from model runs either in a coupled mode or in a stand alone mode forced by observations, in particular precipitation. Due to the lack of global information on soil water and snow depth, model validation is in general performed by comparing predicted runoff with in situ measurements in a number of river basins. Besides, international projects for inter-comparing the global hydrological models have been initiated in the recent years (e.g., PILPS [12]; GSWP1 [13]). However, these approaches remain limited and do not provide a global evaluation of the models accuracy. Thus, direct comparison of models outputs with independent observations, in particular the GRACE-based hydrological products, could be very instructive. However at present, such comparisons first serve to evaluate the precision of the GRACE products. Besides, they will provide the basis for future space data assimilation into the global hydrological models.

This paper presents results of monthly land water change over 2 years (from April 2002 to May 2004) from the GRACE geoids recently released by the GRACE project [2]. The method developed in this study differs from previously published GRACE results [3,14,15] in that it tries to separate mass signals from four different surface reservoirs (soil plus underground plus surface water reservoirs, snow pack, atmosphere and ocean) through an inverse modelling based on generalized least-squares adjustment [16]. The inverse approach which combines the GRACE observations with stochastic properties of the hydrological (or oceanic) signal significantly reduces the recovered land (or ocean) water signal compared to the direct conversion of geoid anomalies into water mass, because of noise reduction and elimination of unrelated signal (e.g., atmospheric noise).

## 2. The GRACE geoids

The data set recently provided to GRACE users by the GRACE project consists of monthly sets of spherical harmonic geoid coefficients (and associated uncertainties), up to degree and order 100, since April 2002. These coefficients derived from raw tracking measurements (GRACE consists of a pair of satellites whose mutual distance, absolute positions and velocities are continuously monitored) are currently computed by two groups: the Center for Space Research (CSR) in the USA and the GeoForschungsZentrum (GFZ) in Germany. The geoid coefficients are corrected for atmospheric loading and oceanic tides. An a priori model for the oceanic variability was also removed during the GRACE data processing. Therefore, temporal changes of the geoid coefficients

mainly represent change in continental water storage, non-tidal oceanic effects and residual atmospheric noise. In this study, we use the CSR geoid data, spanning from April 2002 to May 2004. Fig. 1 displays the temporal coverage of this data set. The length of the horizontal bars corresponds to the numbers of days used to construct each monthly geoid from the raw measurements. Because of too few usable raw measurements, a single monthly geoid is provided for April–May 2002. For 2003, the May geoid is a combination of April plus May data. Although the spherical harmonic coefficients of each monthly geoid are given up to degree and order 100, in this study we follow earlier studies [3,14,15] and only consider harmonic coefficients up to degree 30 (half horizontal wavelength of 660 km). In effect as shown by Tapley et al. [3] and Schmidt et al. [15], at higher degrees – shorter wavelengths – the signal to noise ratio is too low due to residual errors in the data processing that are not yet totally controlled. As in previous studies, we also fix the degree 2, order 0 harmonic (half wavelength of 10 000 km) to zero because of the current large uncertainty associated with this coefficient.

## 3. Methodology

### 3.1. The direct problem

#### 3.1.1. Modelling geoid variations from the different global model forecasts

The static component of the gravity field $G_0$ corresponds to nearly 99% of the total field, mainly due to solid Earth contributions. This term can be easily evaluated and removed by computing the temporal mean of a long enough series of GRACE monthly geoids, or considering a single geoid computed with a long period of time of satellite observations. In this study, the monthly time-variable geoid $\delta G(t)$ is merely computed as the difference between the monthly geoid $G(t)$ measured by GRACE at time $t$, and the static mean field component:

$$\delta G(t) = G(t) - G_0 \quad (1)$$

Using the 20 monthly geoids, we computed a 2-year mean geoid which was further removed to each individual monthly geoid. This allows removal of the static geoid contributions related to the Earth's internal structure as well as to any 'long-term' surface

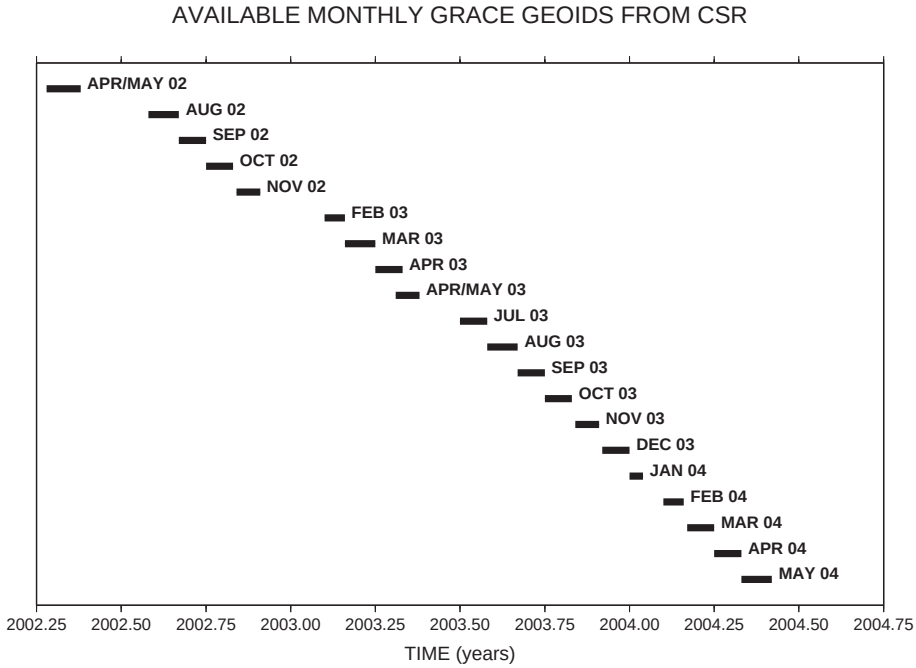


Fig. 1. Temporal coverage of the GRACE geoids provided by CSR (University of Texas) covering the period from 04/2002 to 05/2004 (each bar corresponds to ~1-month time span).

fluid signal (e.g., deep, slowly-varying aquifers) that cannot be extracted with only 2 years of data. Thus, the corresponding geoid differences (also called monthly GRACE geoids in the following) only reflect short-term geoid change associated with surface mass redistributions.

Let $\delta C_{nm}(t)$ and $\delta S_{nm}(t)$ be the "normalized" Stokes coefficients expressed in terms of millimeters of geoid height, where $n$ and $m$ are the degree and order respectively. The time-variable geoid is thus expressed as:

$$\delta G(t) = \sum_{n=1}^{N}\sum_{m=0}^{n}(\delta C_{nm}(t)\cos(m\lambda) + \delta S_{nm}(t)\sin(m\lambda))P_{nm}(\cos\theta) \quad (2)$$

where $N$ is the maximum degree of the decomposition, $\theta$ is the co-latitude, $\lambda$ is the longitude and $P_{nm}$ is the associated Legendre polynomial which is dimensionless. Assuming that the global fluid contributions are not correlated in time and space, we consider that $\delta G(t)$ is the sum of $k=1, 2, \ldots, K$ fluid contributions:

$$\delta G(t) = \sum_{k=1}^{K}\delta G_k(t) = \Omega\delta G \quad (3)$$

where $\Omega$ is the "separating" matrix formed by a column of identity-blocks that ensures the non-correlation between the geoid coefficients of the different fluid contributions. Let $\delta q(t)$ be a surface density associated with surface water mass, expressed in terms of equivalent-water thickness at time $t$, whose harmonic coefficients, $\delta A_{nm}(t)$ and $\delta B_{nm}(t)$, can be used to evaluate the corresponding geoid anomaly coefficients by filtering:

$$\begin{pmatrix}\delta C_{nm}(t)\\ \delta S_{nm}(t)\end{pmatrix} = W_n\begin{pmatrix}\delta A_{nm}(t)\\ \delta B_{nm}(t)\end{pmatrix} \quad (4)$$

where $W_n$ is an isotropic spatial filter that weights the surface density coefficients, and whose analytical expression is [17]:

$$W_n = \frac{2\pi G R_e \rho_W}{(2n+1)\gamma(\theta)}(1+z_n) \quad (5)$$

where $z_n$ represents the Love numbers that enable to take into account the elastic compensation of the Earth to surface load. $\gamma(\theta)$ is the normal gravity on the reference ellipsoid at the co-latitude $\theta$. $G$ ($\sim 6.67\cdot 10^{-11}$ m$^3$ kg$^{-1}$ s$^{-2}$) is the gravitational constant and $R_e$ ($\sim$6378 km) is mean Earth's radius. $\rho_W$ ($\sim$1000 kg m$^{-3}$) is the water density. The latter equation is used to compute the geoid harmonic coefficients from monthly surface density grids $\delta q(\theta, \lambda, t)$ and provided either by global oceanic/hydrological models or atmospheric surface pressure observations. The corresponding Stokes coefficients are defined by [18]:

$$\begin{pmatrix}\delta C_{nm}(t)\\ \delta S_{nm}(t)\end{pmatrix} = \frac{(1+z_n)R_e^2}{(2n+1)M}\iint_S \delta q(\theta,\lambda,t) \times \begin{pmatrix}\cos\\ \sin\end{pmatrix}(m\lambda)P_{nm}(\cos\theta)\delta S \quad (6)$$

since redistributions of fluid mass $\delta q\delta S$ on the surface of the Earth produce variations of the Stokes coefficients, taking the elastic compensation of the Earth's crust into account. $M$ is the total mass of the Earth ($\sim 5.97602\cdot 10^{24}$ kg).

Note that in case of atmospheric surface pressure or ocean bottom pressure $\delta p(\theta, \lambda, t)$ data, commonly expressed in Pa or N/m$^2$, the corresponding surface density variation $\delta q(\theta, \lambda, t)$ is:

$$\delta q(\theta,\lambda,t) = \frac{\delta p(\theta,\lambda,t)}{\rho_W \gamma(\theta)}. \quad (7)$$

In practice, once $\delta q$ is computed for each time step from model outputs using Eqs. (6) and (7), each surface density grid is decomposed into spherical harmonics $\delta A_{nm}(t)$ and $\delta B_{nm}(t)$, and then converted into corresponding geoid coefficients $\delta C_{nm}(t)$ and $\delta S_{nm}(t)$ by applying the direct filtering procedure (Eq. (4)).

These time-series of "model/data" coefficients represent the a priori information that will be used as input in the inversion (described in the next section). For each fluid contribution $k$ and for each time step $t$, it consists of: an initial solution used as "first guess"; an a priori model uncertainty matrix; and a model covariance matrix that described the statistical relationship between the geoid coefficients of a given fluid reservoir $k$ at time $t$.

### 3.1.2. Estimation of the a priori model uncertainties

A priori uncertainties on model harmonic coefficients are derived from statistical comparisons between the geoid coefficients derived from the different oceanic/hydrological models associated with each reservoir $k$. They are simply computed as the

time variances of these coefficients for each month of the year and over the longest time span available. These variances are used as the diagonal elements of the model covariance matrix $C_M$.

*3.1.3. Estimation of the a priori model covariances*

To estimate the model covariance matrix $C_k(t)$ from geoid coefficients, we consider $D_k(\Delta t)$, the matrix formed by the list of all geoid coefficients previously computed for the fluid reservoir $k$ and over a time period $\Delta t$. By construction, the matrix $D_k(\Delta t)$ is such that each row corresponds to a particular month and each column to a given coefficient $\delta C_{nm}(t)$ or $\delta S_{nm}(t)$. Then, the model covariance matrix $C_k(t)$ is simply estimated by computing the product:

$$C_k(t) = [D_k(\Delta t) - \overline{D_k}]^{\mathrm{T}}[D_k(\Delta t) - \overline{D_k}] \tag{8}$$

where $\overline{D_k}$ is the time-mean value of the model coefficients computed during $\Delta t$ months. Several previous tests made by inverting synthetic geoid data have suggested that an optimal value for $\Delta t$ would be the 2–3 months centred around the considered month $t$ (see [1]). Greater values of this time span give rise to numerical smoothing, and thus provide a less precise geoid solution. To estimate the spatial correlations between couples of geoid coefficients of degrees and orders $u$, $v$, $n$, $m$, respectively, the elements of $C_k(t)$ are multiplied by the weighting function $\psi$ defined by:

$$\psi(u,v,n,m) = (2|n-u|+1)^{-1}(2|m-v|+1)^{-1} \tag{9}$$

*3.2. The inverse approach for separating the fluid mass contributions*

The numerical strategy for separating the contributions of the different reservoirs was previously presented in [1]. It is based on the matrix formalism of the generalized least-squares criteria developed by Tarantola [16]. It consists of estimating separately the spherical harmonic coefficients, in terms of equivalent-water heights, of different fluid reservoirs (atmosphere, oceans, soil waters and snow pack) from the monthly GRACE geoids. For each water mass reservoir, the solution is a linear combination of the coefficients measured by GRACE, of the a priori information from climate models and optimal coefficients fitting:

$$\Gamma_k(t) = \Gamma_k^0(t) + C_k\Omega\left(C_D + C_M + \Omega C_k\Omega^{\mathrm{T}}\right)^{-1} \times \left[\Gamma^{\mathrm{OBS}}(t) - \Omega\Gamma_k^0(t)\right] \tag{10}$$

where $\Gamma_k(t)$ is the vector formed by the list of all spherical harmonic coefficients of the geoid to be solved for the $k$-th contribution, $\Gamma^{\mathrm{OBS}}(t)$ is the vector formed with the geoid coefficients from GRACE, $\Gamma_k^0(t)$ corresponds to the initial solution coefficients vector (i.e. "first guess"). $C_D$ and $C_M$ are the a priori covariance matrices of the GRACE geoid coefficients, and of the models, respectively. The latter matrix and the vector $\Gamma_k^0(t)$ are estimated from the geoid coefficients derived from global model outputs for each month (see previous section).

In practice, the matrix to be inverted (terms in parenthesis in Eq. (10)) is symmetric by construction, and often positive definite. We used a strategy of fast Cholesky factorisation to solve this system, instead of a LU decomposition. In extreme conditions of ill-conditioning of the system, we also chose to apply a complete Singular Value Decomposition (SVD) but this is a more time-consuming option.

After solving the linear system (Eq. (10)), the a posteriori covariance matrix $C_k^{\mathrm{POS}}$ is computed using:

$$C_k^{\mathrm{POS}} = C_k - C_k\Omega^{\mathrm{T}}\left(\Omega C_k\Omega^{\mathrm{T}} + C_D + C_M\right)^{-1}\Omega C_k. \tag{11}$$

The a posteriori uncertainties associated to the fitted geoid coefficients of the reservoir $k$ are given by the root-mean square values of the diagonal elements of $C_k^{\mathrm{POS}}$:

$$\sigma_k^{\mathrm{POS}}(t) = \sqrt{C_k^{\mathrm{POS}}(\mathrm{diag})} \tag{12}$$

where "diag" stands for individual-diagonal elements of the a posteriori matrix.

The estimated surface density coefficients $\delta A_{nm}^{\mathrm{POS}}(t)$ and $\delta B_{nm}^{\mathrm{POS}}(t)$, expressed in terms of equivalent-water height, are then estimated by filtering the fitted geoid coefficients $\delta C_{nm}^{\mathrm{POS}}(t)$ and

$\delta S_{nm}^{\mathrm{POS}}(t)$ listed in the solution $\Gamma_k(t)$ of each reservoir $k$ using:

$$\begin{pmatrix} \delta A_{nm}^{\mathrm{POS}}(t) \\ \delta B_{nm}^{\mathrm{POS}}(t) \end{pmatrix} = V_n W_n^{-1} \begin{pmatrix} \delta C_{nm}^{\mathrm{POS}}(t) \\ \delta S_{nm}^{\mathrm{POS}}(t) \end{pmatrix} \quad (13a)$$

with:

$$V_n = \begin{cases} 1 & \text{if } n < n_{\min} \\ \frac{1}{2}\cos\left(\pi \frac{n - n_{\min}}{n_{\max} - n_{\min}}\right) & \text{if } n_{\min} \le n \le n_{\max} \\ 0 & \text{if } n > n_{\max} \end{cases} \quad (13b)$$

where $W_n^{-1}$ is the inverse predicting filter of Eq. (4). It is tapered by a stabilizing function $V_n$ that apodises the amplitudes of $W_n^{-1}$ for degrees between $n_{\min}$ and $n_{\max}$, in order to avoid the development of spurious short-wavelength undulations. Obviously, the main disadvantage of using such a smoothed operator is to remove short-wavelength details in the solution, but this is necessary to avoid numerical instabilities in the matrix inversion of the system (Eq. (10)), and to cancel the effects of noise for high-degrees (typically $n_{\min}=25$ and $n_{\max}=30$).

An iterative process was implemented. Tests have shown that convergence was obtained after ~5 iterations. Thus solutions presented in Section 4 correspond to the 5th iteration.

### 3.3. Model outputs used for the inversion

To construct the "first guess" as well as the $C_k$ covariance matrices, we considered the following models:

#### 3.3.1. Land hydrology

- LaD model [9]
- WGHM model [11]

The Land Dynamics (LaD) model developed by Milly and Shmakin [9] estimates the time-varying storage of snow, root-zone soil water and ground water by solving water and energy balance equations which relate temporal change in storage to rainfall, snowfall, evapotranspiration, sublimation, snow melt, soil water drainage and ground water discharge to streams. The model provides $1^\circ \times 1^\circ$ monthly global grids of snow, root-zone soil water, underground waters (from the shallow and dynamic unconfined saturated zone) for 1981–2003.

The Water GAP Global Hydrology Model (WGHM) [11] was specifically designed to estimate river discharge for water resources assessments. It computes $0.5^\circ \times 0.5^\circ$ gridded time series of monthly runoff and river discharge and is tuned against time series of annual river discharges measured at 724 globally distributed stations. Other products of the model are monthly gridded time series of water storage in the snow cover, soil water within the root zone, ground water and surface water stored in rivers, lakes and wetlands. The data are available for 2002 to 2004.

#### 3.3.2. Ocean bottom pressure

We used ocean bottom pressure data derived from two Ocean Global Circulation Models (OGCMs):

- POCM-4C (Parallel Ocean Circulation Model) [19,20]
- ECCO [21]

While initial resolutions and time spans of ocean bottom pressure grids provided by these models are different, we interpolated the data onto $1^\circ \times 1^\circ$ grids and constructed a climatology (standard year).

#### 3.3.3. Atmosphere

Atmospheric loading effects were removed during the GRACE data processing. However, in order to account for any residual atmospheric signal in the GRACE geoid, we considered a 'residual atmosphere' reservoir for the inversion. Thus, to construct the corresponding covariance matrix, we used gridded differences between two atmospheric surface pressure data sets: NCEP [22] and ECMWF.

These gridded differences were further developed into spherical harmonics, and corresponding coefficients, in units of equivalent water height were further expressed in terms of geoid height (see [1]).

### 3.4. Deriving time-series of water mass variations from monthly geoids: test results

As indicated above, we separated the contributions of four different equivalent-water mass reservoirs: soil plus underground plus surface waters reservoir (called 'liquid reservoir' in the following), snow pack, resi-

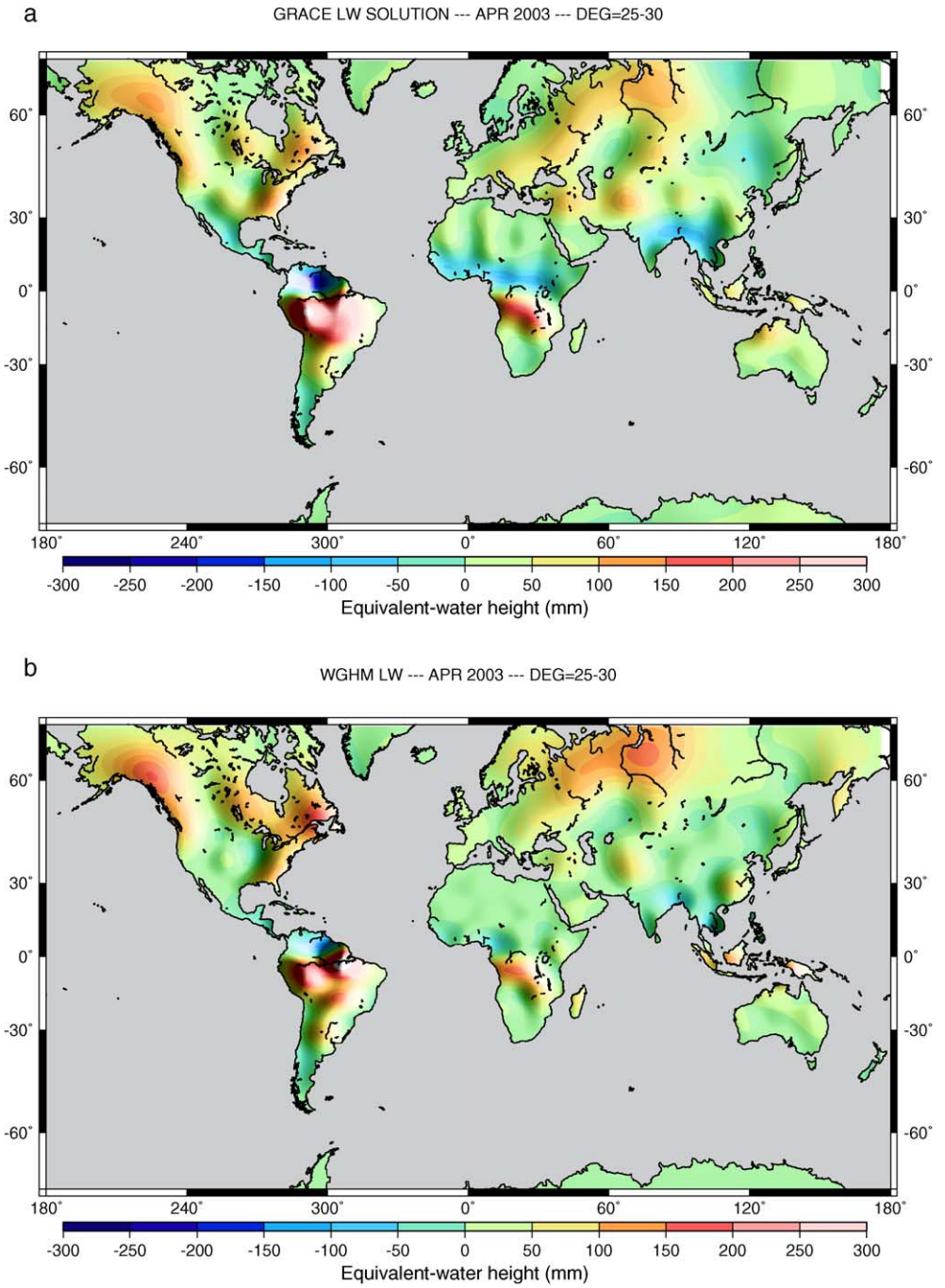


Fig. 2. (a) Land water solution for April 2003 for the nominal case after 5 iterations; (b) WGHM land water storage for April 2003; (c) log of errors for the input geoid (upper curve), model (middle curve) and nominal solution (lower curve) for April 2003, as a function of harmonic degree; (d) difference in land water storage between GRACE and WGHM; (e) residual geoid for April 2003; (f) land water solution after 10 iterations with first guess set to zero, (g) convergence curves for the nominal case and first guess set to zero.

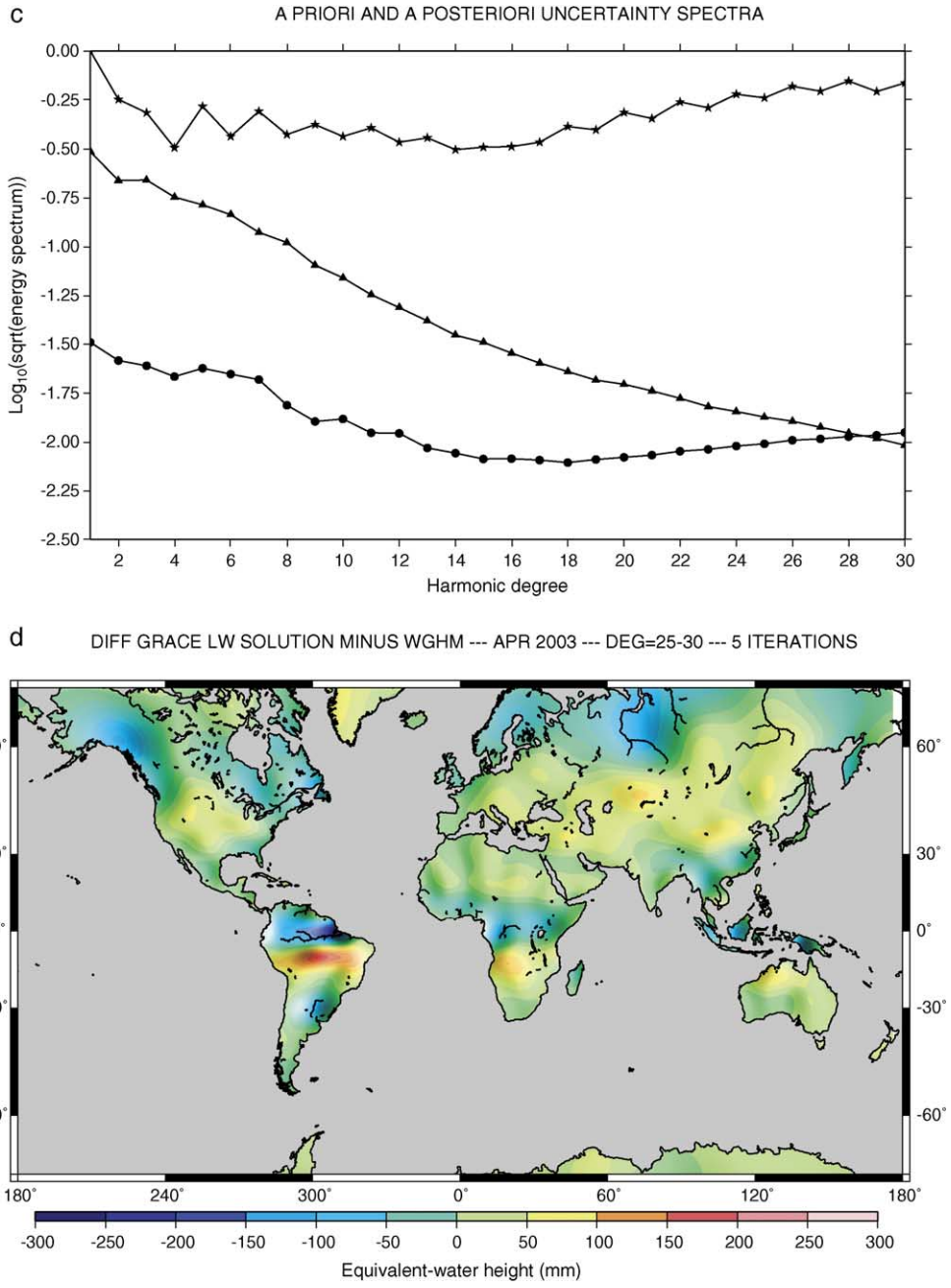


Fig. 2 (*continued*).

dual atmosphere and ocean, from each of the 20 months (from April/May 2002 to May 2004). For constructing the 'first guess' as well as the model covariance and model error matrices, the following models have been considered for defining the 'nominal' case: ECCO for the ocean bottom pressure, the difference ECMWF minus NCEP for the residual atmospheric signal, and WGHM for land waters (liquid water reservoirs and snow pack). The nominal land water solution (sum of liquid waters plus snow

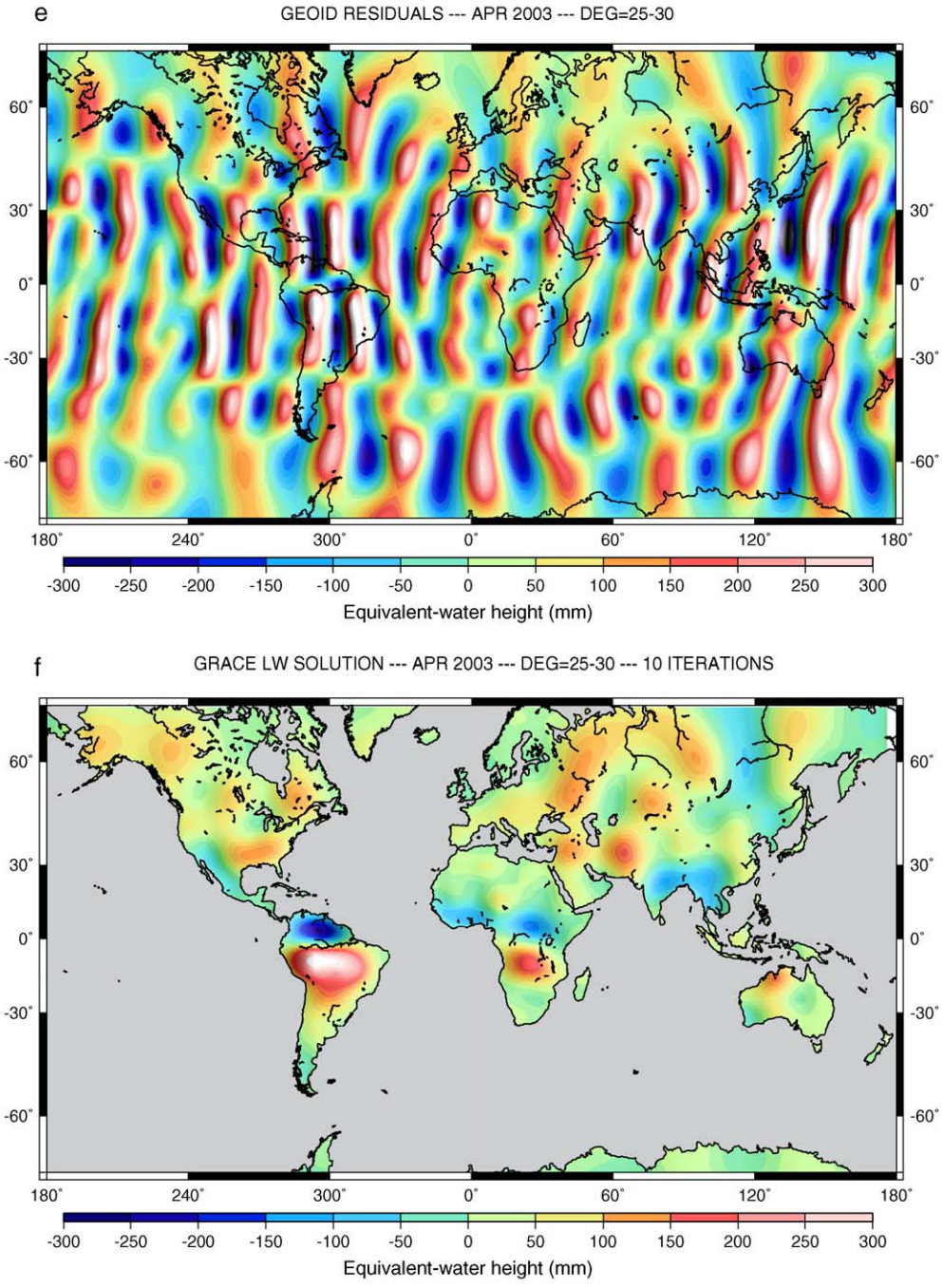


Fig. 2 (*continued*).

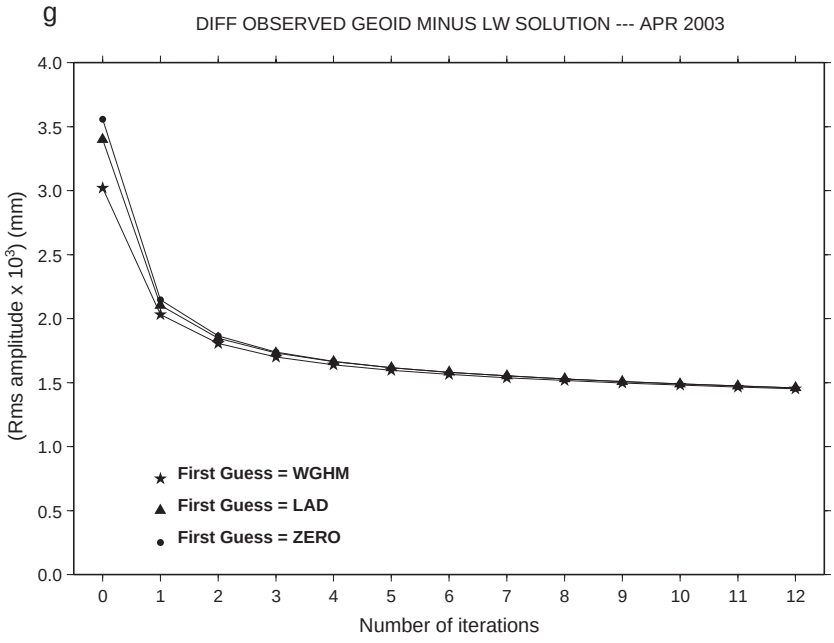


Fig. 2 (*continued*).

mass), up to degree 30, for April 2003, based on the inversion of the GRACE geoid, is presented in Fig. 2a. It corresponds to the solution obtained after 5 iterations, when convergence was reached. For comparison, the WHGM prediction (sum of all water components) – up to degree 30 – is shown in Fig. 2b. The error spectra as a function of harmonic degree for the input geoid, the solution and the model are plotted in Fig. 2c. We note that the a posteriori errors of the solution are smaller (almost by a factor 10) than the model errors and GRACE input geoid errors. The a posteriori errors decrease with increasing degree up to degree 15, and then increase progressively, following the spectrum behaviour of a priori observed uncertainties. Fig. 2d and 2e show maps of the differences between the GRACE solution and the model, and the residual geoid based on the difference between the GRACE geoid and the geoid solution constructed using the solutions of the inversion for the four reservoirs (total soil water, snow, residual atmosphere and ocean). Fig. 2d shows positive signal in a number of regions, in particular over the Amazon basin, an indication that the GRACE solution contains more power than predicted by the model. The residual geoid map (Fig. 2e) is dominated by north–south strips of amplitude in the range $\pm$ 300 mm (equivalent water height). These strips are also seen in the input GRACE geoid and may result from a combination of noise and Gibbs oscillations associated with the spherical harmonic cut-off at degree 30. The fact that the residual geoid presents the same strips as in the input geoid is comforting. It means that the GRACE geoid noise was not incorporated into the solution and that the inversion process was efficient.

We further performed a series of tests – for April 2003 – to evaluate the robustness of the solution. The discussion here is limited to the land water storage solution. The tests concern different first guesses (for land water storage) as input (WGHM and LaD, and an extreme case with the first guess set to zero), an error-free model assumption (a priori covariance matrix $C_M$ set to zero), a model error larger than the nominal case (covariance matrix $C_M$ elements multiplied by 100), data errors set to zero, etc. The land water solution for the error-free model case is almost identical to the nominal solution while the large model error case provides a solution very close to the first guess (WGHM solution). The case with no error in the data gives rise to a very noisy (high-amplitude north–south strips) in the land water solution. Finally

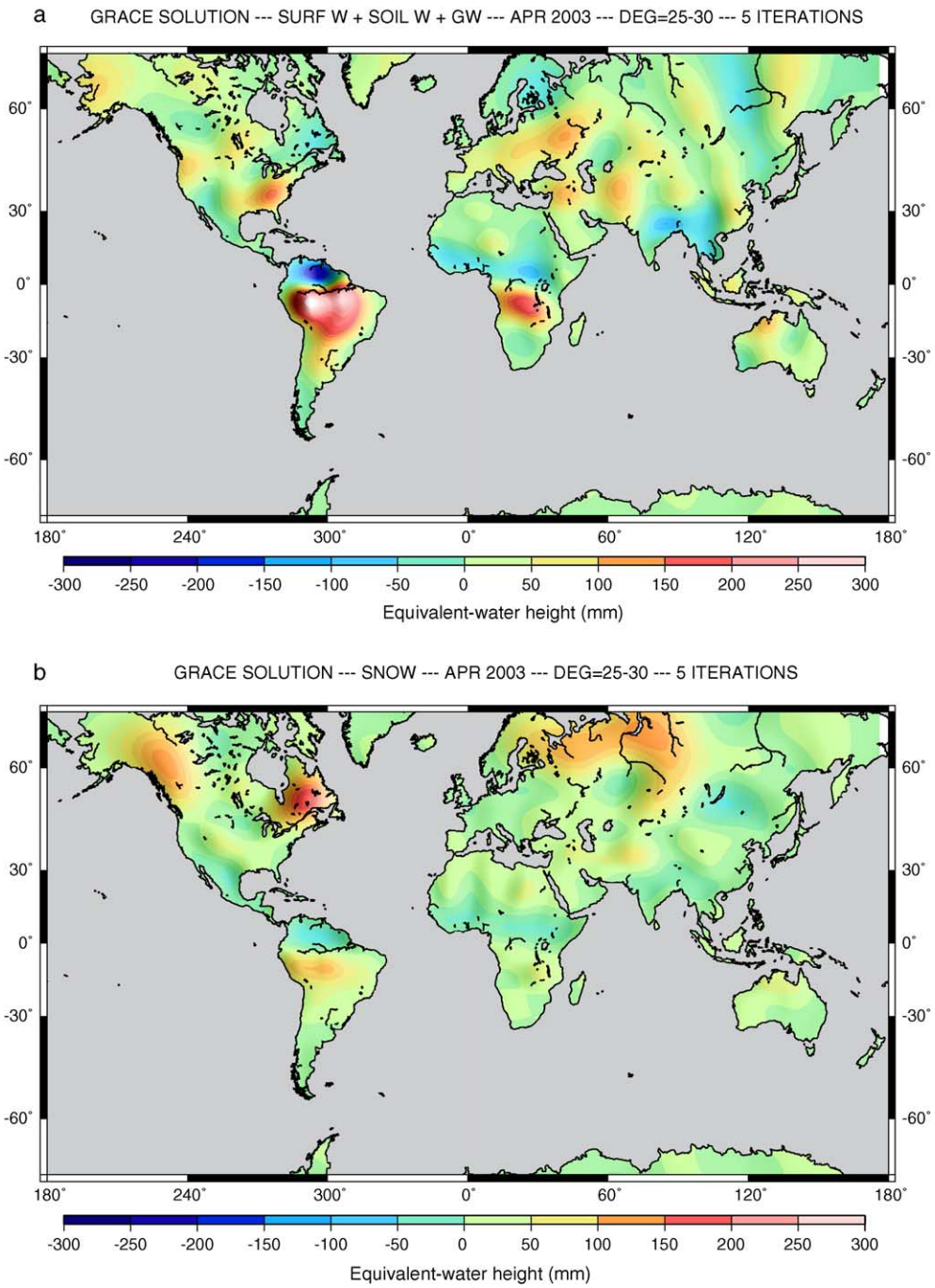


Fig. 3. Example of an efficient separation of hydrological components for April 2003 (5-iteration solutions, degree maximum 25–30): (a) total (liquid) water solution (surface waters + soil moisture + groundwater) and (b) snow depth solution.

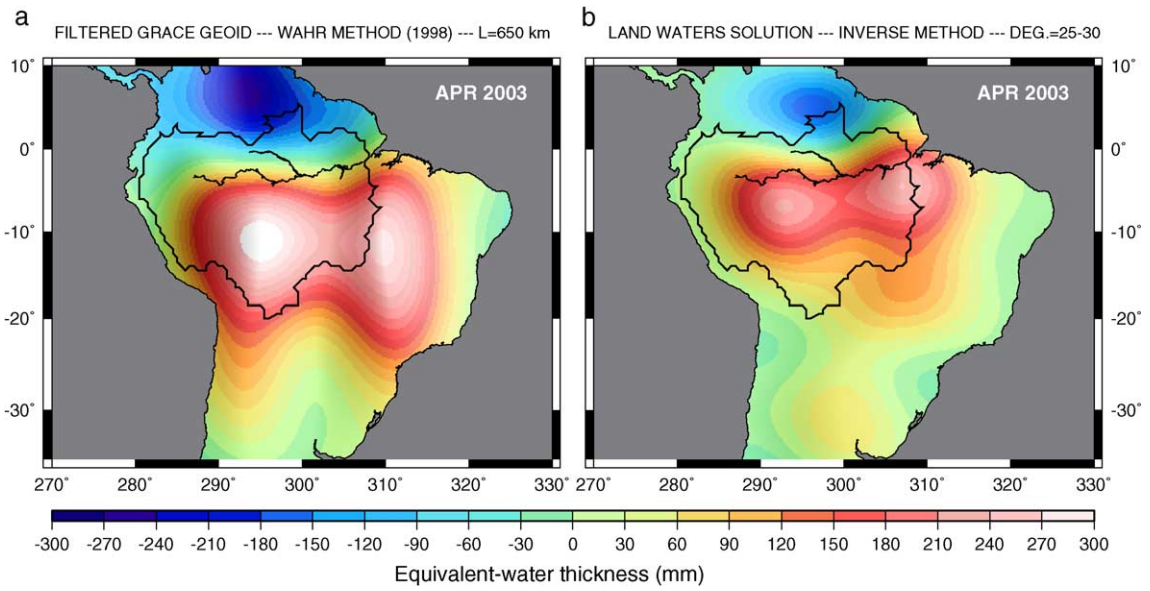


Fig. 4. Continental water storage variations over the Amazon basin for April 2003 derived using two approaches: (a) linear filtering from Wahr and Molenaar [4] ($L$=650 km); (b) land water solution after 5 iterations using the proposed inverse method.

the case with first guess set to zero is interesting. After one iteration, the solution shows the familiar pattern of the nominal solution and model but the amplitudes of the water mass anomalies are on the average a factor of 2 smaller. After 10 iterations, the solution displays anomalies amplitudes in good agreement with the nominal case (Fig. 2f). We note, however, that the solution is slightly smoother (less short wavelength signal) than in the nominal case. This point needs further investigation. Finally, Fig. 2g presents the root mean square residuals between the GRACE geoid and the reconstructed geoid, as a function of iteration rank, for the nominal case, a case with LaD as first guess, and the case with the first guess set to zero. As expected, the convergence is slower when the first guess is set to zero. However, the three cases provide similar convergence behaviour after ~5 iterations.

We next present the individual solutions for liquid water (soil plus underground plus surface reservoirs) (Fig. 3a) and solid water (snow pack) (Fig. 3b). It appears that the inversion process does rather well in separating the liquid and solid water components, even though we note some contaminating signal in the snow map over the Amazon basin, which evidently should not be there. This means that some improvement in the inversion method is still needed.

### 3.5. Comparison with the results provided by the Wahr et al. [4] method

The approach we propose differs from the Wahr et al. filtering by the fact it is an inversion, which combines different a priori information (i.e. model forecasts, errors and GRACE observations) to improve iteratively a "first guess". The solution is linearly corrected by GRACE data through covariance matrices in space and time.

Early work of Jekeli [23] inspired Wahr and Molenaar [4] to propose a method based on the Gaussian averaging of the Stokes coefficients observed by GRACE to remove the effects of the noise at high harmonic degrees. Given the half-height length $L$, the Jekeli's smoothing operator $J$ versus degree $n$ is defined by an iterative relation:

$$J_0 = \frac{1}{2\pi}, J_1 = \frac{1}{2\pi}\left[\frac{1+\mathrm{e}^{-2b}}{1-\mathrm{e}^{-2b}}\right],$$
$$J_{n+1} = -\frac{2n+1}{b}J_n + J_{n-1} \qquad (14)$$

where the parameter $b$ is:

$$b = \frac{\ln 2}{1-\cos(L/R_\mathrm{e})}. \qquad (15)$$

This filtering was also used by Tapley et al. [3] and Schmidt et al. [15] to compute the maps of the continental water storage changes from monthly GRACE geoids. These studies used a value of 750 km (degree 27) for $L$ as a good compromise between spatial resolution and effect of noise. Wahr and Molenaar [4] predicting filter $W_n$ to derive coefficients of equivalent-water from the geoid anomaly ones is:

$$W_n = \frac{3\rho_W(1+z_n)}{\rho_e(2n+1)} \tag{16}$$

where $\rho_e$ is the mean Earth's density (~5517 kg/m$^3$). This latter operator is numerically equivalent to the one defined earlier in Eq. (5).

Fig. 4 presents results in the region of Amazon basin comparing this approach and ours over the Amazon basin for April 2003. For the Wahr et al. method, we used $L=650$ km, which corresponds to our cut-off harmonic degree (degree 30).

Amplitudes of the two maps are comparable, and range between $\pm 300$ mm of equivalent-water height. However, differences are regionally important (the rms difference is 86.83 mm over the Amazon basin), and mainly due to a shift of the principal maxima of the water storage changes from one solution to the other. The inversion-derived solution shows more short-wavelength details, with the positive anomaly in closer agreement with the model predictions (see Fig. 2), more centred over the basin and less leakage on the oceanic areas.

## 4. Land water solutions from GRACE: results

### 4.1. Time series of monthly solutions

Six of the 20 monthly solutions for the total land water storage (sum of liquid water storage plus snow) are presented in Fig. 5a–f. These six maps correspond to the months of July 03, September 03, November 03, January 04, March 04 and May 04. The 20 solutions are based on the nominal case discussed in Section 3. Because the year 2003 is almost complete (only January and June are lacking), compared to the other 2 years, we restrict our discussion to that particular period. The largest signals are observed in large tropical river basins (Amazon and Orinoco basins in South America, Congo and Niger basins in Africa, Ganges and Bramhaputra basins in India) as well as in several river basins of the northern hemisphere (Mississippi basin in North America, Ob and Lena rivers basins in northeast Asia, Volga basin in eastern Europe). In high latitude regions, month to month changes are also clearly visible (Alaska, eastern and western Canada, northern Asia). In these high latitude regions, the observed signal results from the combined contributions of total soil water and snow. In general, the solutions agree well with the models as far as the geographical positions of the anomalies are concerned. In terms of relative amplitude, the solutions differ significantly from the models however, as do the models each other. We note however a better agreement with WGHM than with LaD (not shown). We computed maps of the differences between the GRACE solutions (total soil water plus snow) and the WGHM model (not shown, except for April 2003; see Fig. 2c). Amplitude differences of individual months can reach up to $\pm 100$ mm in terms of water height. Comparisons with the individual solutions and model predictions indicate that there is no systematic underestimation by the model. It clearly depends on the region.

### 4.2. Seasonal cycle

From the individual monthly solutions available, we have constructed a seasonal cycle solution.

For that purpose, we assumed that the GRACE-derived changes of water continental mass $\delta q(\theta, \lambda, t)$ are the sum of a linear trend, a seasonal sinusoid (which pulsation is $\omega = \frac{2\pi}{T}$, with $T \sim 1$ year) and water mass residuals $\delta q^{RES}(\theta, \lambda, t)$:

$$\delta q(\theta,\lambda,t) = [\alpha(\theta,\lambda)t + \beta(\theta,\lambda)] + [\xi(\theta,\lambda)\cos(\omega t + (\theta,\lambda))] + \delta q^{RES}(\theta,\lambda,t) \tag{17}$$

The parameters which we adjusted for each grid point $(\theta, \lambda)$ are the linear trend (i.e. slope $\alpha(\theta, \lambda)$ and $\beta(\theta, \lambda)$), and then the seasonal cycle (i.e. amplitude $\xi(\theta, \lambda)$ and phase $\varphi(\theta, \lambda)$) after being corrected from the temporal trend. For this purpose, we used a least-squares fitting to solve the system:

$$\delta Q = \Phi \cdot X \tag{18}$$

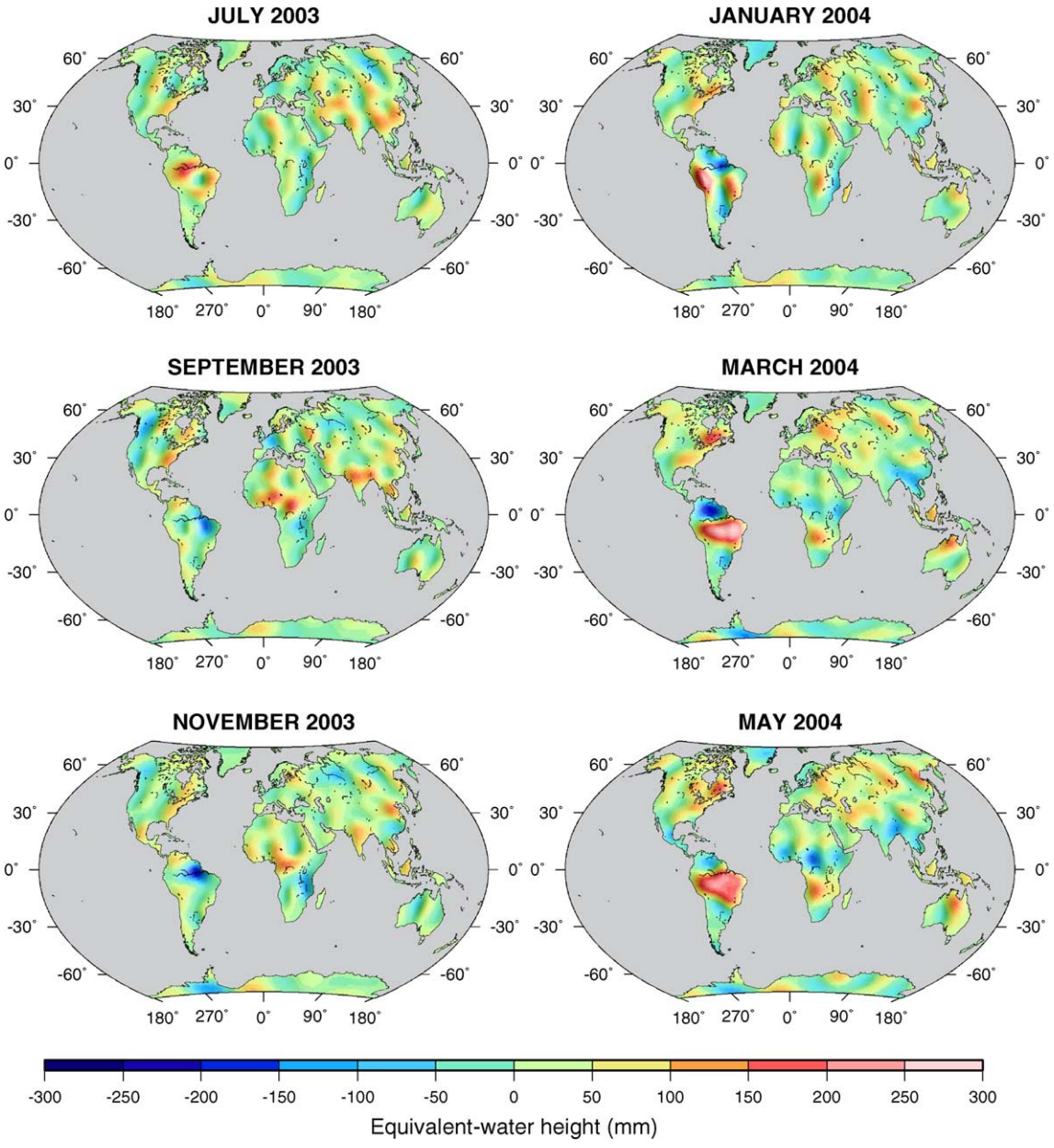


Fig. 5. Monthly land waters (sum of liquid water reservoirs and snow pack) solutions (after 5 iterations) for 6 months of the 20 computed solutions (nominal case).

where the vector $\delta Q$ is the list of the GRACE-derived LW values, $\Phi$ and $X$ are the configuration matrix and the parameter vector, respectively. The latter two terms are successively:

$$\Phi = \lfloor t_j \quad 1 \rfloor, \text{ and } X = [\,\alpha \quad \beta\,] \tag{19}$$

for adjusting the temporal trend, and:

$$\Phi = \lfloor \cos(\omega t_j) \;\; \sin(\omega t_j) \rfloor, \text{ and } X = [\,\xi\cos\varphi \;\; -\xi\sin\varphi\,] \tag{20}$$

for fitting the seasonal amplitude and phase at each grid point. In both cases, according to the least-

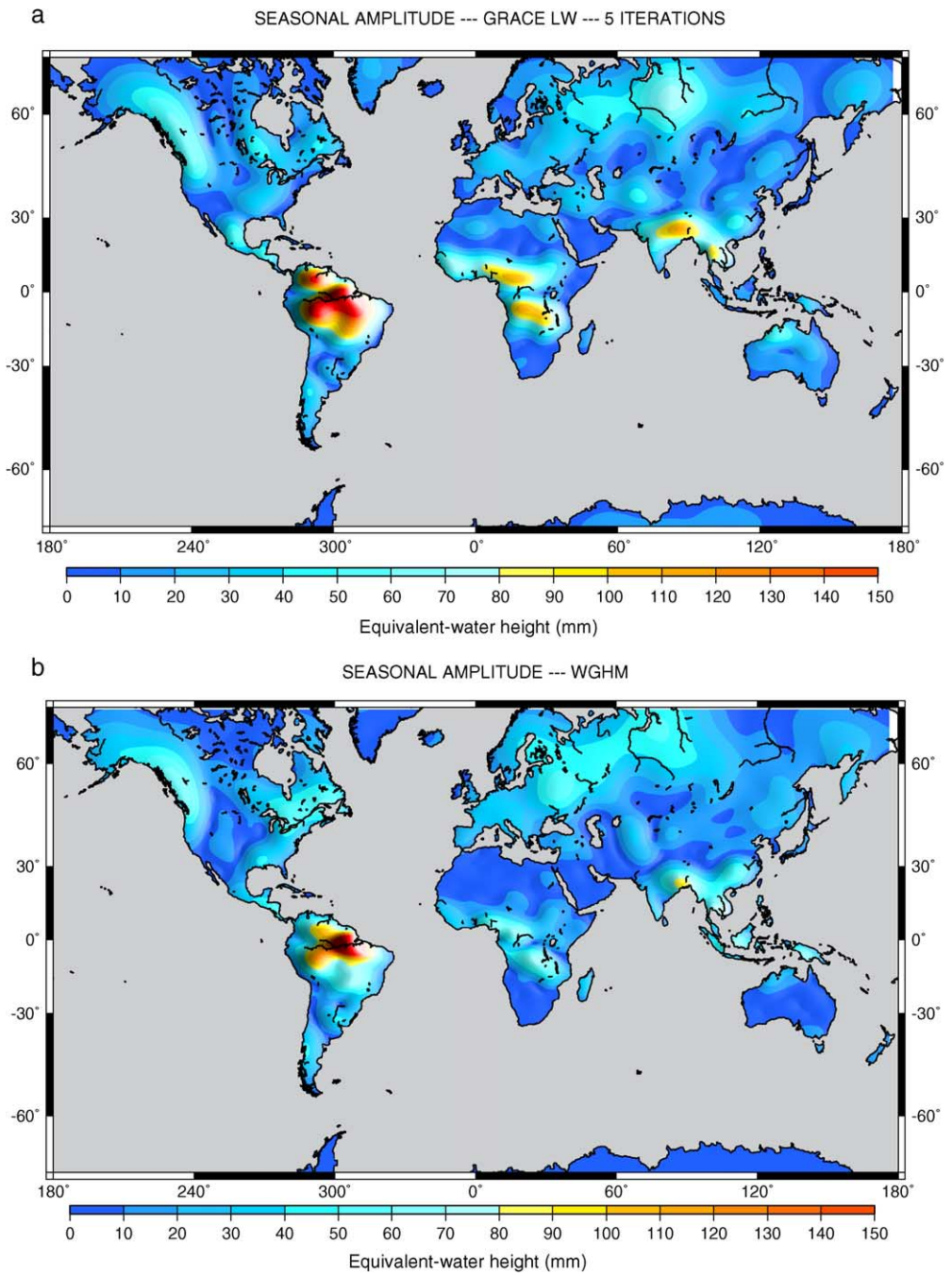


Fig. 6. Results of the least-squares adjustment of the seasonal amplitudes: (a) for land water storage from GRACE; and (b) for the WGHM model.

squares criteria, the solution vector of the system is:

$$X^{\mathrm{SOL}} = \left(\Phi^{\mathrm{T}}\Phi\right)^{-1}\Phi^{\mathrm{T}}\delta Q \tag{21}$$

The amplitude maps of the observed and model seasonal cycles are presented in Fig. 6a and b.

Looking at Fig. 6a and b, we note that the GRACE seasonal cycle presents in some regions higher amplitude than WGHM, principally in the tropical river basins. In South America, the maximum GRACE signal is located at the southern edge of the Amazon river while in the model, it coincides with the river. Moreover, the GRACE seasonal amplitude map clearly shows a large signal over the Orinoco basin, not seen in WGHM.

We further looked at the interannual signal. We first considered several couples of similar months of years 2002, 2003 and 2004 and computed the differences. In these cases, the signal is evidently smaller than at the seasonal time scale, but clear inter-annual anomalies are visible over several basins of the northern hemisphere (e.g., the Ob and Lena basins in Siberia) as well as over tropical basins (Orinoco, Amazon, Niger, Congo and Ganges).

## 5. Time-series of water volume change in large river basins

At a given month $t$, the regional variation of water volume $\delta V(t)$ over a given river basin $S$ is the sum of the products of the GRACE-derived surface load $\delta q_j$, with $j=1, 2, \ldots$ (expressed in terms of equivalent-water height) inside $S$, by the elementary surface $R_e^2\delta\lambda\delta\theta\sin\theta_j$:

$$\delta V(t) = R_e^2\delta\lambda\delta\theta\sum_{j\in S}\delta q_j(\theta,\lambda,t)\sin\left(\theta_j\right) \tag{22}$$

where $\delta\lambda$ and $\delta\theta$ are the sampling grid steps along longitude and latitude, respectively. In practice, the points of $S$ used in Eq. (22) are extracted over eight drainage basins located in the tropics (Amazon, Orinoco, Tocantins, Parana, Congo, Niger, Ganges and Mekong). The contour of each basin is based on masks of 0.5° resolution from Oki and Su [24]. The locations of the eight drainage basins are presented in Fig. 7. Fig. 8 displays the temporal water volume change – spatially averaged – over each basin for the 2 years. The predicted volume change from the WGHM model is also shown. We note in general good amplitude agreement with the model predictions for some basins: Amazon, Orinoco, Congo, Mekong.

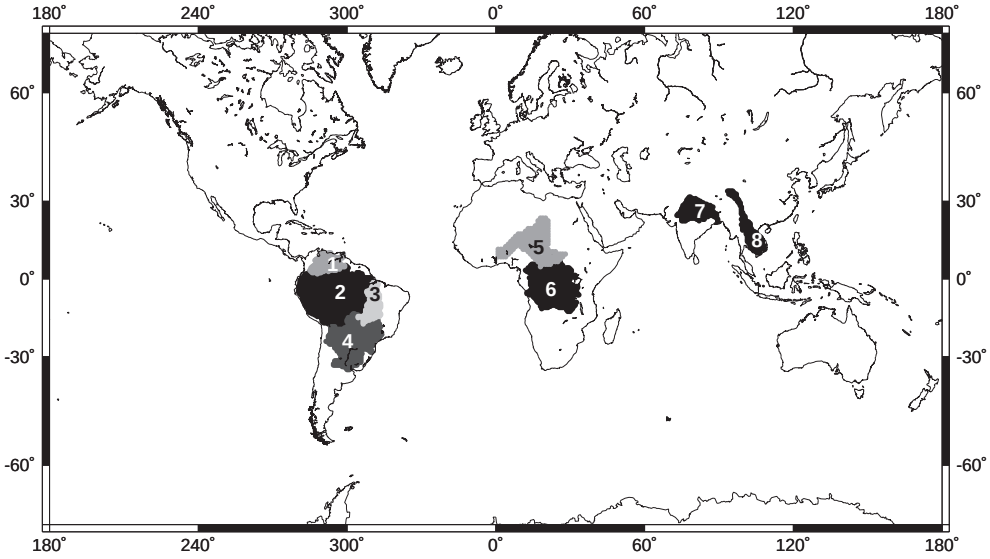


Fig. 7. Location maps of the eight studied drainage basins. 1: Orinoco; 2: Amazon; 3: Tocantins; 4: Parana; 5: Niger; 6: Congo; 7: Ganges; 8: Mekong.

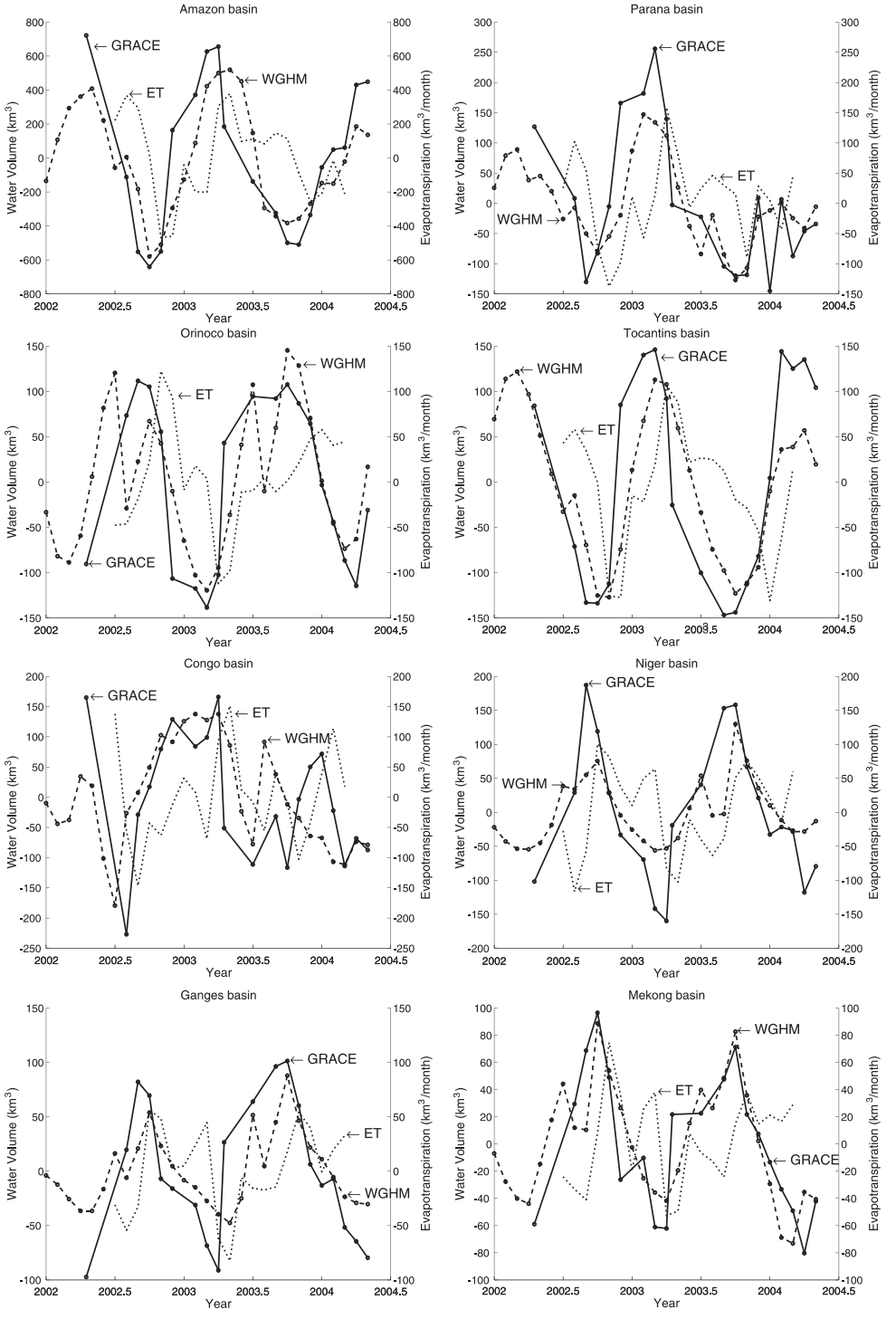


Fig. 8. Time series of total water volume (average over the basin area) based on GRACE (solid curve), on the WGHM model (dashed curve) and estimate the mean evapotranspiration (dotted curve), for each of the eight studied basins.

For the Tocantins and Parana basins, the GRACE-derived water volumes are larger than model predictions. Poor agreement is noticed for the Ganges and Niger basins. Additional model comparisons need to be performed in the future.

We further attempted to provide an estimate of the mean evapotranspiration for each basin. For that purpose, we considered the water mass budget equation:

$$\frac{dV}{dt} = P - E - R \quad (23)$$

with $V$: land water storage, $P$: precipitation, $E$: evapotranspiration, $R$: runoff. We computed the derivative, $dV/dt$, of the water volume change using the GRACE solutions, subtracted the precipitation $P$ averaged over the basin (using data from the Global Precipitation Climatology Centre [25,26]), and further subtracted the mean runoff $R$ over the basin using outputs of the WGHM model. Finally we estimated the evapotranspiration $E$. For each basin, mean (i.e., averaged over the basin area) evapotranspiration curve is superimposed to the observed and model volume curves in Fig. 8. Evapotranspiration is a key-component of hydrological budget at the local/regional scale. This parameter is presently poorly described due to lack of measurements and modelling complexity. Werth and Avissar [27] summarize the contradictions of several datasets of Amazonian evapotranspiration: Global Climate Models tend to produce an evapotranspiration cycle that follows the precipitation cycle – mostly during the rainy austral summer (December–February) and less during drier austral winter (June–August) – whereas models of evapotranspiration derived from observations of net surface radiation and atmospheric humidity provide a weak annual cycle that is out of phase with that of precipitation. Note however that the estimates of the mean evapotranspiration presented here for the Amazon basin are in relatively good agreement with the NCEP-derived evapotranspiration reported in [27], both in phase and amplitude. From the results presented in Fig. 8, we note that over equatorial basins (i.e. Amazon, Congo), the annual cycle is not well marked whereas a strong annual cycle is present in the tropical basins (i.e., Parana, Orinoco, Tocantins, Niger, Ganges and Mekong). Besides, the annual cycle of evapotranspiration appears correlated with the precipitation cycle in the latter regions. Over the Amazon basin, the annual mean evapotranspiration rate is of 600 km$^3$/month or 3.3 mm/day. These values can be compared with the modelled and observational estimates of Costa and Foley [28] who have found respectively 3.66 and 3.27 mm/day for the whole basin, 4.18 and 4.12 over the rain forest.

## 6. Conclusion

In this study, we present new solutions of time variations in continental water storage from the available GRACE geoids, over the period April 2002 to May 2004. These solutions, with a spatial resolution of 660 km, are based on a generalized least-squares inversion that combines different model and data errors information. The iterative version of the inversion scheme rapidly converges towards a unique land water solution. Moreover, the algorithm efficiently filters out the spurious undulations present in the input GRACE geoids. However, resolution and precision of the computed land water maps still need to be improved, hopefully when uncertainties on the observed GRACE coefficients (especially beyond degree 30) will be reduced. From monthly land water time series, we also estimate the temporal variation of the mean evapotranspiration over eight large drainage basins located in the tropics. It is based on the water balance equation and the use of observed precipitation and predicted runoff data. Since evapotranspiration remains a poorly known hydrological parameter (because neither well-measured nor modelled), its estimate based on monthly land water maps derived from GRACE represents an interesting contribution to global hydrology.

The entire series of maps of the 20 monthly “Land Waters” solutions can be downloaded from our laboratory web site: http://www.obs-mip.fr/umr5566/.

## Acknowledgements

We thank the GRACE project for having made available the monthly GRACE geoids. We also thank C. Milly, P. Döll and J. Alcamo for providing us with global outputs of their hydrological models, as well as A. Tarantola and an anonymous reviewer for helpful comments. One of us (FF) benefited from a CNES-ALCATEL SPACE PhD grant.

## References


[1] G. Ramillien, A. Cazenave, O. Brunau, Global time-variations of hydrological signals from GRACE satellite gravimetry, Geophys. J. Int. 158 (2004) 813–826.

[2] B.D. Tapley, S. Bettadpur, M. Watkins, C. Reigber, The gravity recovery and climate experiment: mission overview and early results, Geophys. Res. Lett. 31 (2004) L09607, doi:10.1029/2004GL019920.

[3] B.D. Tapley, S. Bettadpur, J.C. Ries, P.F. Thompson, M. Watkins, GRACE measurements of mass variability in the Earth system, Science 305 (2004) 503–505.

[4] J. Wahr, M. Molenaar, Time variability of the Earth's gravity field: hydrological and oceanic effects and their possible detection using GRACE, J. Geophys. Res. 103 (B12) (1998) 30205–30229.

[5] M. Rodell, J.S. Famiglietti, Detectability of variations in continental water storage from satellite observations of the time dependent gravity field, Water Resour. Res. 35 (9) (1999) 2705–2723.

[6] N.I. Ducoudré, K. Laval, A. Perrier, SECHIBA, a new set of parameterizations of the hydrologic exchanges at the land atmosphere interface within the LMD Atmospheric General Circulation Model, J. Clim. 6 (2) (1993) 248–273.

[7] H. Douville, E. Bazile, P. Caille, D. Giard, J. Noilhan, L. Peirone, F. Taillefer, Global Soil Wetness Project: forecast and assimilation experiments performed at Meteo-France, J. Meteorol. Soc. Jpn. 77 (1999) 305–316.

[8] H. Douville, F. Chauvin, Relevance of soil moisture for seasonal climate predictions; a preliminary study, Clim. Dyn. (2000) 16719–16736.

[9] P.C.D. Milly, A.B. Shmakin, Global modeling of land water and energy balances: 1. The Land Dynamics (LaD) model, J. Hydrometeorol. 3 (2002) 283–299.

[10] T. Ngo-Duc, J. Polcher, K. Laval, A 53-year forcing data set for land-surface models, J. Geophys. Res. 110 (2005) D06116, doi:10.1029/2004JD005434.

[11] P. Döll, F. Kaspar, B. Lehner, A global hydrological model for deriving water availability indicators: model tuning and validation, J. Hydrol. 270 (2003) 105–134.

[12] Y. Shao, A. Henderson-Sellers, Modeling soil moisture: a project for intercomparison of land surface parameterization schemes Phase 2(b), J. Geophys. Res. 101 (1996) 7227–7250.

[13] P.A. Dirmeyer, A. Dolman, N. Sato, The pilot phase of the Global Soil Wetness Project, Bull. Am. Meteorol. Soc. 80 (1999) 851–878.

[14] J. Wahr, S. Swenson, V. Zlotnicki, I. Velicogna, Time-variable gravity from GRACE: first results, Geophys. Res. Lett. 31 (2004) L11501, doi:10.1029/2004GL019779.

[15] R. Schmidt, F. Flechtner, Ch. Reigber, P. Schwintzer, A. Güntner, P. Doll, G. Ramillien, A. Cazenave, S. Petrovic, H. Jochman, J. Wunsch, GRACE observations of changes in continental water storage, Glob. Planet. Change (in press) 18, doi: 10.1016/j.gloplacha.2004.11.018.

[16] A. Tarantola, Inverse Problem Theory, Elsevier, Amsterdam, 1987, 613 pp.

[17] G. Ramillien, Gravity/magnetic potential of uneven shell topography, J. Geod. 76 (2002) 139–149, doi:10.1007/s00190-002-0193-5.

[18] W.H. Heiskanen, H. Moritz, Physical Geodesy, W.H. Freeman and Co, San Francisco, 1967.

[19] D. Stammer, R. Tokmakian, A. Semtner, C. Wunsch, How well does a 1/4° global circulation model simulate large-scale oceanic observations? J. Geophys. Res. 101 (1996) 25799–25811.

[20] R. Tokmakian, Comparisons of time series from two global models with tide-gauge data, Geophys. Res. Lett. 23 (1996) 3759–3762.

[21] D. Stammer, C. Wunsch, R. Giering, C. Eckert, P. Heimbach, J. Marotzke, A. Adcroft, C.N. Hill, J. Marshall, The global ocean circulation during 1992–1997, estimated from ocean observations and a general circulation model, J. Geophys. Res. 107 (C9) (2002) 3118, doi:10.1029/2001JC000888.

[22] R.E. Kistler, et al., The NCEP–NCAR 50-year reanalysis: monthly means CD-ROM and documentation, Bull. Am. Meteorol. Soc. 82 (2001) 247–267.

[23] C. Jekeli, Alternative Methods to Smooth the Earth's Gravity Field, Rep. 327. Dep. of Geod. Sci. and Surv., Ohio State Univ., Columbus, 1981.

[24] T. Oki, Y.C. Su, Design of Total Runoff Integrating Pathways (TRIP)—a global river channel network, Earth Interact. 2 (1) (1998) 1–37.

[25] B. Rudolf, H. Hauschild, W. Rueth, U. Schneider, Terrestrial precipitation analysis: operational method and required density of point measurements, in: M. Desbois, F. Desalmond (Eds.), Global Precipitations and Climate Change, NATO ASI Series I, vol. 26, Springer-Verlag, 1994, pp. 173–186.

[26] B. Rudolf, T. Fuchs, U. Schneider, A. Meyer-Christoffer, Introduction of the Global Precipitation Climatology Centre (GPCC), Deutscher Wetterdienst, Offenbach a.M., p. 16.

[27] D. Werth, R. Avissar, The regional evapotranspiration of the Amazon, J. Hydrometeorol. 5 (2004) 100–109.

[28] M.H. Costa, J.A. Foley, Water balance of the Amazon Basin: dependence on vegetation cover and canopy conductance, J. Geophys. Res. 102 (D20) (1997) 23973–23989.